PERGAMON

International Journal of Heat and Mass Transfer 45 (2002) 1271–1285

International Journal of HEAT and MASS TRANSFER

www.elsevier.com/locate/ijhmt

Prediction of swirling confined diffusion flame with a Monte Carlo and a presumed-PDF-model

S. Repp [a], A. Sadiki [a,*], C. Schneider [a], A. Hinz [b], T. Landenfeld [b], J. Janicka [a]

[a] *Fachgebiet Energie- und Kraftwerkstechnik, Technische Universität Darmstadt, Petersenstrasse 30, 64287 Darmstadt, Germany*
[b] *Robert Bosch GmbH, Germany*

Received 7 December 2000; received in revised form 15 June 2001

Abstract

This work aims to compare numerical results obtained by using the Monte Carlo composition-PDF method and a presumed-β-PDF in order to reveal their effects on the prediction of flow and scalar fields in swirling confined methane diffusion flame. Using the intrinsic low dimensional manifolds method for modelling the chemistry and a second moment closure for the turbulence, it is shown that both PDF-methods provide a similar accuracy level of the prediction of mean quantities. While the presumed-β-PDF performs using reasonable computational efforts, the Monte Carlo-PDF allows to capture well the turbulence–chemistry interaction and strong finite-chemistry effects such as local extinction. © 2002 Published by Elsevier Science Ltd.

Keywords: Prediction; Turbulence–chemistry interaction; Swirling confined flame; PDF methods; Combustion; Swirling; Turbulence

1. Introduction

Two major objectives in modern design of technical combustion systems, in which heat and mass transfer play a central role, are optimisation of combustion efficiency and reduction of pollutants, such as nitric oxides or carbon monoxide. In order to meet these requirements, the application of computational fluid dynamics (CFD) has become a popular tool for predicting flow phenomena and therefore for designing complex three-dimensional flow systems as i.e. combustion chambers of gas turbines [2] in which swirling flows are indispensable. Characterised by recirculation of hot combustion products along with strong turbulence–chemistry effects, swirling confined reacting flows belong to the important and challenging tasks in modern CFD.

Different approaches to describe the nonlinear nature of turbulence–chemistry interaction capturing finite-chemistry effects for the accurate prediction of pollutants can be found in the literature. All approaches use turbulent combustion models which make use of statistical properties of the scalar field.

Solving for the transport equation of the probability density function (PDF) [32] represents an attractive approach, because it contains the full statistical information. The transport equations for either the joint composition PDF (all considered species mass fractions and temperature) can then be solved, or the joint velocity–composition PDF is solved [14,33,34]. Using the Monte Carlo methods may be the only computationally efficient manner. While a major advantage of this approach is the closed representation of the chemical source term, it suffers from significant computing time and storage expenses as well as other modelling imperfections for the molecular diffusion. In general, reduced chemistry has to be used since the computational expenses are proportional to the number of species mass fractions in the PDF. Because of uncertainties in modelling the molecular diffusion, it may be regarded most applicable when molecular diffusion is not very important, such as in flames with slow chemistry at low Damköhler numbers.

Most of the published Monte Carlo scalar-PDF simulations nowadays are applied to comparatively

* Corresponding author. Tel.: +49-6151-16-2757; fax: +49-6151-16-6555.
E-mail address: sadiki@hrz2.hrz.tu-darmstadt.de (A. Sadiki).

0017-9310/02/$ - see front matter © 2002 Published by Elsevier Science Ltd.
PII: S0017-9310(01)00243-5

Nomenclature

C_i $\{i = 1, 2, 3, 4, b, s, \mu, \chi\}$	model coefficients
C_ε, C_{ε_i} $\{i = 1, 2, 3\}$	dissipation equation model coefficients
C_{ijk}	turbulent transport tensor
D	diffusion coefficient
f	mixture fraction
$\tilde{k}$	turbulent kinetic energy
l	turbulent length scale
MPG_{ij}	density–velocity-fluctuations correlation
P	probability density function (PDF)
P_ϕ	probability density function of quantity ϕ
P_{ij}	production tensor
S_α	source term of species α
S	swirl number
R	radius
Re	Reynolds number
T	temperature
t	time
$\mathbf{u}, u_i$	velocity vector
u, v, w	axial, radial, tangential component of velocity
$\widetilde{u_i'' u_j''}$	Reynolds stress tensor
$\dot{w}_\alpha$	chemical reaction rate of species α
$x_j = \{x, y, z\}$	Cartesian coordinate vector
Y_α	mass fraction of species α

Greek symbols

β	beta-PDF
δ_{ij}	Kronecker delta
$\tilde{\varepsilon}$	dissipation rate of turbulent kinetic energy
ν	kinematic viscosity
μ	dynamic viscosity
Π_{ij}	pressure–strain correlation
ρ	mass density
σ	Schmidt number
φ, ϕ	arbitrary scalar quantity

Subscripts and superscripts

α	species α
t	turbulent
$'$	difference from conventional mean value
$''$	difference from Favre mean value

Symbols

$\overline{}$	conventional mean value
$\widetilde{}$	Favre averaged mean value
$\langle\,\rangle$	expected value
$\langle\,|\,\rangle$	conditioned mean quantity

simple flame configurations. Only few simulations of technical combustion systems have been carried out [1,6], however, on the basis of the assumption of chemical equilibrium for the reactions. Another way of turbulence–chemistry coupling applies a Linear Eddy Model which is a method of simulating molecular mixing on a one-dimensional domain embedded in a turbulent flow. This method accounts for the small-scale turbulent dynamics in order to construct a joint-PDF instead of assuming its shape [10,20].

Alternatively, the shape of the PDFs can be presumed implying the solution of the transport equations of the parameterisation variables, such as mean and variance of certain quantities [11,16]. The functions for the shape of the PDF depend in general on these statistical moments of the composition space variables [25]. Nevertheless, up to now mostly one-dimensional presumed-PDFs have been widely used [17] and combined with equilibrium chemistry or the laminar flamelet model. In the laminar flamelet model, the thermochemical state is determined by the mixture fraction and a second parameter that takes into account non-equilibrium chemistry [28,29]. The mixture fraction statistics are usually approximated by calculating the mean mixture fraction and its variance by modelled transport equations. The PDF of the mixture fraction is then constructed by assuming a certain shape, for example a clipped Gauss function or a β-function depending on the mean and the variance of the compositions space variables as parameters. The mean thermochemical variables are calculated using this PDF and the (nonlinear) relationships that exist between the mixture fraction and the instantaneous thermochemical variables. This concept allows then to avoid the evaluation of the mean reaction rates, which is the central problem here. Valid for flames in which fast chemistry is predominant, it naturally treats molecular diffusion including differential diffusion effects if the model does not fail in predicting the behaviour of the mixture fraction. It predicts therefore flame structures well but fails for minor components formed by slow chemical processes. This problem is overcome by the unsteady flamelet model [31] on the expense of larger computational effort. Conditional moment closure [4] is also an attractive approach

applicable to arbitrarily complex chemistry mechanisms, but it entails an increased dimensionality of the interaction problem.

Gutheil and Bockhorn [11] have constructed a three-dimensional joint PDF based on clipped Gaussian distribution, whose shape is defined by a large set of parameters. Janicka and Kollmann [16] have calculated mean radial concentrations in diffusion flames using a two variable formalism. They have applied several shapes for the PDF, namely combinations of β- and δ-functions.

If required, the turbulence is taken into account in all these approaches through turbulence models separately implemented in an appropriate CFD code. Many authors have presented various complete models in the past. Jones and Kakhi [18] combined a k–ε turbulence model and a full Reynolds stress model with a scalar Monte Carlo approach, respectively, to compute a turbulent methane–air jet diffusion flame. Chen et al. [5] used a second-order turbulence model in combination with a five-variable PDF. Focused on the description of the chemistry mechanism by using the laminar flamelet method and the so-called intrinsic low dimensional manifolds (ILDM) approach, a presumed-PDF method and a Monte Carlo-PDF (MC-PDF) approach have been accounted for in [12,13,22].

It must be observed that, the lower moments of the PDF variables, serving as input values for the multivariate presumed-PDF model used in [13], have not been presented. Furthermore, no systematic comparison of the coupling models has been carried out for confined configurations. Indeed, in [13] a CFD-code with a nonlinear turbulence model of second order (SSG model) has been coupled to the PDF-subcode by using a post-processing interaction approach, so that only the impact of the chemistry mechanism on the species concentration and temperature could be accounted for. To investigate the impact of the turbulence–chemistry interaction on flow and scalar fields, an iterative exchange approach is rather needed.

The present work is therefore focused on a comparison of PDF methods in order to investigate the impact of turbulence–chemistry interaction modelling on the prediction of flow and scalar fields in swirling confined reacting flows. In other words, this comparison is meant to analyse the difference that can be expected when utilising two different computational coupling models for the description of turbulence–chemistry interaction. From a theoretical point of view, emphasis is put on the validation of a presumed-β-PDF model by means of the MC-PDF method.

2. Applied models

In general, a complete statistical model for the description of turbulent flames consists of a turbulence closure and a chemistry mechanism; these two are combined by an appropriate closure assumption for the treatment of the turbulence-chemistry interaction.

2.1. Turbulence closures

The Favre-averaged Navier–Stokes equations are closed by solving the unknown Reynolds stress tensor on a second order level of closure. In the physical modelling and in simulation, this enables to capture the strong streamline curvature and recirculation of the investigated reacting flow. For solving the transport equations of the Reynolds stress tensor, $\widetilde{u_i'' u_j''}$, in its statistically stationary case, the linear model of Jones and Musonge [19] in its revised form [17] is used for the pressure–strain correlation, Π_{ij}, in contrast to the nonlinear SSG-model used in [13]. The density–velocity-fluctuations correlation, MPG_{ij}, is modelled with well-established assumptions [30] and the model of Daly and Harlow [8] is applied for the unknown turbulent transport term, C_{ijk}.

Throughout the paper, the variables $x_k, \tilde{u}_j, \tilde{k}, \tilde{\varepsilon}, \overline{\rho}, \overline{p}$ and ν represent spatial coordinates, Favre-averaged velocity, Favre-averaged quantities of turbulent kinetic energy and dissipation rate, mean density, mean pressure and kinematic viscosity. The quantity u_j'' represents the Favre-fluctuating part of the velocity and P_{ij} is the production of $\widetilde{u_i'' u_j''}$. δ_{ij} is the Kronecker delta.

Because of self-consistency of the paper, let us summarize these closure relations whilst the model coefficients used are given in Table 1.

$$\Pi_{ij} = -C_1 \overline{\rho}\tilde{\varepsilon}\left(\frac{\widetilde{u_i'' u_j''}}{\tilde{k}} - \frac{2}{3}\delta_{ij}\right) + C_2 \delta_{ij}\overline{\rho}\widetilde{u_l'' u_m''}\frac{\partial \tilde{u}_l}{\partial x_m} - C_3\overline{\rho}P_{ij} + C_4\overline{\rho}\tilde{k}\left(\frac{\partial \tilde{u}_i}{\partial x_j} + \frac{\partial \tilde{u}_j}{\partial x_i}\right)$$

Table 1
Turbulence and scalar flux model coefficients

Coefficient	Value
C_1	3.0
C_2	0.44
C_3	0.46
C_4	0.23
C_{ε_1}	1.4
C_{ε_2}	1.9
C_{ε_3}	0.95
C_ε	0.18
C_s	0.22
C_b	0.2326
C_μ	0.09
σ_z	0.7
$\sigma_{z''^2}$	0.7
C_χ	2.0

$$-\frac{2}{3}C_4\overline{\rho}\tilde{k}\frac{\partial\tilde{u}_k}{\partial x_k}\delta_{ij}-\left(\frac{3}{2}C_2+C_3\right)\times\left(\overline{\rho}\widetilde{u_l''u_j''}\frac{\partial\tilde{u}_l}{\partial x_i}+\overline{\rho}\widetilde{u_l''u_i''}\frac{\partial\tilde{u}_l}{\partial x_j}\right), \quad (1)$$

$$MPG_{ij}=-C_b\frac{\tilde{k}}{\overline{\rho}\tilde{\varepsilon}}\left(\widetilde{u_j''u_k''}\frac{\partial\overline{\rho}}{\partial x_k}\frac{\partial\overline{p}}{\partial x_i}+\widetilde{u_i''u_k''}\frac{\partial\overline{\rho}}{\partial x_k}\frac{\partial\overline{p}}{\partial x_j}\right),$$

$$C_{ijk}=-C_s\frac{\tilde{k}}{\tilde{\varepsilon}}\overline{\rho}\widetilde{u_k''u_l''}\frac{\partial\widetilde{u_i''u_j''}}{\partial x_l}. \quad (2)$$

In these relations, the turbulence dissipation rate is assumed to be isotropic and determined from its evolution equation of the form

$$\frac{\partial(\overline{\rho}\tilde{\varepsilon}\tilde{u}_j)}{\partial x_j}=-C_{\varepsilon_1}\overline{\rho}\frac{\tilde{\varepsilon}}{\tilde{k}}\widetilde{u_i''u_j''}\frac{\partial\tilde{u}_i}{\partial x_j}-C_{\varepsilon_2}\overline{\rho}\frac{\tilde{\varepsilon}^2}{\tilde{k}}+C_{\varepsilon_3}\frac{\tilde{\varepsilon}}{\tilde{k}}\overline{\rho'u_i''}\times\frac{\partial\overline{p}}{\partial x_i}+\frac{\partial}{\partial x_j}\left(\overline{\rho}\nu\frac{\partial\tilde{\varepsilon}}{\partial x_j}+C_\varepsilon\overline{\rho}\frac{\tilde{k}}{\tilde{\varepsilon}}\widetilde{u_j''u_k''}\frac{\partial\tilde{\varepsilon}}{\partial x_k}\right). \quad (3)$$

2.2. Mixing and chemical models

The chemical mechanism is obtained using a description based on ILDM [26,38–40]. Applying an eigenvalue analysis of the chemistry mechanism, only the locally slowest time scales are considered for the approximation of the chemistry mechanism. In this work, the full mechanism and details for the ILDM reduced mechanism for CH_4–air system are described according to Schmidt et al. [38]. A three-scalar mechanism emerges from this procedure, which results in look-tables with coordinates associated with the representative scalars being the mixture fraction f (assuming equal diffusivity) and two reaction progress variables, namely the mass fractions of carbon dioxide and water, Y_{CO_2} and Y_{H_2O}, respectively. All interesting information (e.g. the chemical composition, chemical rates of formation, temperature and density) is therefore stored in the tables as a function of the mixture fraction and the reaction progress variables only.

Provided a current state in scalar space then parameterised by the vector $\boldsymbol{\phi}=(f,Y_{CO_2},Y_{H_2O})$, the motion along the two-dimensional manifold is given by the rate of change of the reaction progress variables. From a chemical point of view, the two reaction progress variables are both reaction products which are correlated. Note that the description via two reaction progress variables is equivalent to a global two-step mechanism except for the advantage of using locally always the two slowest, hence most appropriate, reactions. Hence, during the CFD simulation transport equations of the means and variances of the reaction progress variables

$$\frac{\partial(\overline{\rho}\tilde{Y}_\alpha\tilde{u}_j)}{\partial x_j}=\frac{\partial}{\partial x_j}\left(\overline{\rho}D\frac{\partial\tilde{Y}_\alpha}{\partial x_j}-\overline{\rho}\widetilde{u_j''Y_\alpha''}\right)+\overline{\dot{w}}_\alpha, \quad (4)$$

$$\frac{\partial(\overline{\rho}\tilde{u}_i\widetilde{Y_\alpha''^2})}{\partial x_i}=\frac{\partial}{\partial x_i}\left(\overline{\rho}D\frac{\partial\widetilde{Y_\alpha''^2}}{\partial x_i}\right)-2\overline{\rho}\widetilde{u_i''Y_\alpha''}\frac{\partial\widetilde{Y}_\alpha}{\partial x_i}-\frac{\partial(\overline{\rho}\widetilde{u_iY_\alpha''^2})}{\partial x_i}-\underbrace{\overline{\rho}D\frac{\partial\widetilde{Y_\alpha''}}{\partial x_i}\frac{\partial\widetilde{Y_\alpha''}}{\partial x_i}}_{\tilde{\chi}_\alpha}+2\overline{Y_\alpha''\dot{w}_\alpha''} \quad (5)$$

are solved. Transport of mixture fraction f and variance $\widetilde{f''^2}$ is described by the same equations with the source term being identical zero. Scalar fluxes are modelled with eddy viscosity assumptions of the form

$$-\overline{\rho}\widetilde{u_iz''}=\overline{\rho}\frac{C_\mu\tilde{k}^2/\tilde{\varepsilon}}{\sigma_z}\frac{\partial\tilde{z}}{\partial x_i}\quad\text{and}$$
$$-\overline{\rho}\widetilde{u_iz''^2}=\overline{\rho}\frac{C_\mu\tilde{k}^2/\tilde{\varepsilon}}{\sigma_{z''^2}}\frac{\partial\widetilde{z''^2}}{\partial x_i}\quad(z=f,Y_\alpha) \quad (6)$$

while the scalar dissipation is modelled assuming a constant time scale ratio

$$\tilde{\chi}_\gamma=C_\chi\frac{\tilde{\varepsilon}}{\tilde{k}}\widetilde{z''^2}\quad(\gamma=f,\alpha). \quad (7)$$

Note that contrary to [13], the value $\sigma_z=0.7$ appears to be appropriate here (see Table 1).

To determine the mean quantities $\overline{\rho}$, $\overline{\dot{w}_\alpha}$, and $\overline{Y_\alpha''\dot{w}_\alpha''}$ occurring in these equations, besides the knowledge about the chemical kinetics in the flame one requires statistical information about the influence of turbulent processes on these kinetics, because these terms are highly nonlinear dependent on the composition of the gas mixture and temperature.

2.3. Interaction models

In this study two different ways to implement the ILDM model within a PDF approach with respect to the coupling to the turbulent flow fields are considered. The multivariate presumed-PDF model and the transport equation of the joint composition-PDF solved by using a Monte Carlo-method.

As details of these methods are available in the literature [13,22], only a summary overview is given.

2.3.1. Multivariate presumed-PDF model

In order to account for the turbulence-chemistry interaction a three-dimensional PDF defined via a presumed joint-PDF approach can be applied. The Favre-averaged value of some arbitrary quantity φ is obtained by multiplying the quantity with the mass weighted PDF, $\tilde{P}$, and integrating over composition space according to

$$\tilde{\varphi} = \int\int\int \varphi(f, Y_{CO_2}, Y_{H_2O}) \tilde{P}(f, Y_{CO_2}, Y_{H_2O}) \mathrm{d}f \, \mathrm{d}Y_{CO_2} \, \mathrm{d}Y_{H_2O}. \tag{8}$$

In order to carry out the integration according to Eq. (8), the unknown three-dimensional joint-PDF, $\tilde{P}(f, Y_{CO_2}, Y_{H_2O})$, needs to be modelled adequately. By means of

$$Y^{\star}_{CO_2} = \frac{Y_{CO_2}}{Y_{CO_2,eq}(f)} \quad \text{and} \quad Y^{\star}_{H_2O} = \frac{Y_{H_2O}}{Y_{H_2O,eq}(f)}, \tag{9}$$

a normalised formulation of the reaction progress variables is introduced, whereby $Y_{\alpha,eq}(f)$ refers to the value of these variables at chemical equilibrium for a given mixture fraction [7].

A major advantage of applying the normalisation following Eq. (9) is that the domain of definition of the reaction progress variables is extended to the interval $[0,1]$, allowing for the use of β-functions and the numerical integration over a rectangular domain. Assuming statistical independence between mixture fraction f and the normalised reaction progress variables $Y^{\star}_{\alpha}$, one can then construct a joint-PDF by multiplication of one-dimensional PDFs. Of course, this assumption is a hard approximation between $Y^{\star}_{CO_2}$ and $Y^{\star}_{H_2O}$. There is ample experimental work about turbulent flames that demonstrates that this assumption is not valid, see in [10,11]. We do not attempt to prove the contrary. However, we investigate to what extent such an assumption can help to improve the numerical efficiency required for industrial purposes by comparing the results obtained with Monte Carlo simulation results; thus, the use of a more elaborate ansatz was not performed in this state of the work. Therefore, Eq. (8) can be rewritten as

$$\tilde{\varphi} = \int_0^1 \int_0^1 \int_0^1 \varphi\left(f, Y^{\star}_{CO_2}, Y^{\star}_{H_2O}\right) \times \tilde{P}_{\beta}(f) \tilde{P}_{\beta}(Y^{\star}_{CO_2}) \tilde{P}_{\beta}\left(Y^{\star}_{H_2O}\right) \mathrm{d}f \, \mathrm{d}Y^{\star}_{CO_2} \, \mathrm{d}Y^{\star}_{H_2O}. \tag{10}$$

Since the β-PDFs in Eq. (10) depend merely on the mean and variance of their prescribed variables, the turbulent thermochemical state of the flame is defined by six parameters, namely $\tilde{f}$, $\widetilde{f''^2}$, $\tilde{Y}^{\star}_{CO_2}$, $\widetilde{Y^{\star''2}_{CO_2}}$, $\tilde{Y}^{\star}_{H_2O}$ and $\widetilde{Y^{\star''2}_{H_2O}}$. For an efficient computation of mean values, the numerical evaluation of Eq. (10) is carried out in a preprocessing step generating a six-dimensional look-up table. The implementation in the CFD code is realised by solving the transport equations for the mean and variance of f, Y_{CO_2} and Y_{H_2O} described above.

In order to access the look-up table, a transformation of the Favre-averaged reaction progress variables to their normalised counterpart is necessary during the numerical procedure. This is obtained according to Landenfeld [21] by using the approximate relations

$$\widetilde{Y^{*}_{\alpha}} = Y_{\alpha} \widetilde{\frac{1}{Y_{\alpha,eq}}} \approx \tilde{Y}_{\alpha} \left(\widetilde{\frac{1}{Y_{\alpha,eq}}} \right), \tag{11}$$

$$\widetilde{Y^{*''2}_{\alpha}} = \left(\widetilde{\frac{Y_{\alpha}}{Y_{\alpha,eq}}} \right)^2 - \left(\widetilde{\frac{Y_{\alpha}}{Y_{\alpha,eq}}} \right)^2 \approx \left(\widetilde{Y^{''2}_{\alpha,eq}} + \widetilde{Y^{''2}_{\alpha}} - 2\sqrt{\widetilde{Y^{''2}_{\alpha,eq}}} \sqrt{\widetilde{Y^{''2}_{\alpha}}} \right) \left(\widetilde{\frac{1}{Y_{\alpha,eq}}} \right)^2, \tag{12}$$

with $(1/\widetilde{Y_{\alpha,eq}})$, $(1/\widetilde{Y_{\alpha,eq}})^2$ and $\widetilde{Y^{''2}_{\alpha,eq}}$ also being computed via Eq. (10).

The approximation in (11) is motivated by the lack of information about the neglected term. Keeping this fact in mind, expression (12) is obtained by considering the departure from the equilibrium values through $Y_{\alpha} = Y_{\alpha,eq} - \Delta$ with Δ as departure parameter, then approximating

$$\left(\widetilde{\frac{\Delta}{Y_{\alpha,eq}}} \right)^{''2} \approx \widetilde{\Delta^{''2}} \left(\widetilde{\frac{1}{Y_{\alpha,eq}}} \right)^2,$$

and finally re-writing the departure parameter in terms of Y_{α} and $Y_{\alpha,eq}$. These approximations are substantial, but reasonable for the purpose.

The instantaneous value, S_{α}, of the chemical rate of change of Y_{α} is first read from the ILDM table. Finally, the chemical source terms of Eqs. (4) and (5) are computed via Eq. (10) yielding

$$\overline{\dot{w}}_{\alpha} = \overline{\rho} \tilde{S}_{\alpha,\text{look-up table}} \quad \text{and} \quad \overline{Y''_{\alpha} \dot{w}''_{\alpha}} = \overline{\rho} \left(\widetilde{Y_{\alpha} S_{\alpha}} - \tilde{Y}_{\alpha} \tilde{S}_{\alpha} \right)_{\text{look-up table}}. \tag{13}$$

After implementing the ILDM model within the PDF approach, these mean chemical source terms and the mean density are then fed back to the CFD code.

Thus, the numerical procedure consists of an iterative exchange of the turbulent flow and mixing field, the mean density and the chemical source terms between the CFD code and the PDF subcode. The mean values and variances of the mixture fraction and reaction progress variables obtained from the solution of the corresponding transport equations are used as the input parameters for the look-up table interpolation. This table interpolation provides then the mean values of the density and the chemical source terms required in the transport equations of the reaction progress variables and their variances to be used in the next iteration step.

2.3.2. Monte Carlo-PDF model

Solving for the transport equation of the composition joint-PDF [32,41] represents an elaborate approach for capturing turbulence-chemistry interaction with the major advantage that the chemical source term appears in closed form. Using a Monte Carlo method, the PDF is approximated by an ensemble of notional particles representing a set of Dirac functions in composition

space. The transport equation of the mass weighted PDF $\tilde{P}_\phi(\boldsymbol{\psi};\mathbf{x},t)$, defined in scalar space $\boldsymbol{\psi}$ and in physical space $\mathbf{x}$, as well as in time t, reads

$$\begin{aligned}\overline{\rho}\frac{\partial\tilde{P}_\phi(\boldsymbol{\psi};\mathbf{x},t)}{\partial t}+\overline{\rho}\tilde{u}_j\frac{\partial\tilde{P}_\phi(\boldsymbol{\psi};\mathbf{x},t)}{\partial x_j}+\frac{\partial}{\partial\psi_\alpha}\\ \times[\overline{\rho}S_\alpha\tilde{P}_\phi(\boldsymbol{\psi};\mathbf{x},t)]\\ =-\frac{\partial}{\partial x_j}[\overline{\rho}\langle u_j''\,|\,\boldsymbol{\phi}=\boldsymbol{\psi}\rangle\tilde{P}_\phi(\boldsymbol{\psi};\mathbf{x},t)]\\ -\frac{\partial}{\partial\psi_\alpha}\left[\left\langle-\frac{\partial J_k^\alpha}{\partial x_k}\,\middle|\,\boldsymbol{\phi}=\boldsymbol{\psi}\right\rangle\tilde{P}_\phi(\boldsymbol{\psi};\mathbf{x},t)\right].\end{aligned}\tag{14}$$

The expression $\langle a\,|\,b\rangle$ denotes the mean of quantity a conditioned on the event b. The terms on the left-hand side represent the transient term, the convective term as well as the chemical source term, respectively. On the right-hand side of Eq. (14), turbulent diffusion and mixing in scalar space are captured. Attention is drawn to the closed formulation of the chemical source term S_α. Within the solution algorithm each of the notional particles develops according to these processes using a fractional timestep method [24].

The convective and turbulent diffusive processes are treated via a finite-volume discretisation in physical space. Chemical reactions are described with the ILDM method, hence every particle is assigned with the random variable vector $\boldsymbol{\phi}=(f,Y_{CO_2},Y_{H_2O})$. The unclosed conditional expectation of the velocity fluctuation is closed by means of a simple gradient diffusion approximation

$$\langle u_j''\,|\,\boldsymbol{\phi}=\boldsymbol{\psi}\rangle\tilde{P}_\phi=-\frac{\nu_t}{\sigma_p}\frac{\partial\tilde{P}_\phi}{\partial x_j},\quad \nu_t=C_\mu\frac{\tilde{k}^2}{\tilde{\varepsilon}},\tag{15}$$

with the turbulent Schmidt number $\sigma_p=0.7$ and $C_\mu=0.09$. The mixing process is approximated with the Modified Curl's model [15] consisting of a pairwise interaction of a number of randomly selected particles. Since the primary aim of the present work is to gain insight into the effect of the PDF-modelling approaches to describe the turbulence-chemistry interaction in swirling confined flows, the use of more advanced models such as the EMST [36] or the Binomial Langevin Model [37] was regarded as not justified.

The mean velocity and the turbulent quantities must be externally provided. A first way is to perform the Monte Carlo simulation in a post-processing step as done in [13]. There, the velocity and turbulence fields stem from the computation using ILDM chemistry and the presumed joint-PDF and serve as an input for the Monte Carlo simulation. In this case, the density evaluated from the Monte Carlo computation is not fed back to the CFD calculation. Leaving the flow field unchanged in this way would allow the investigation of the impact of the chemistry mechanism on the species concentrations and temperature. We follow in the present work a second, different way in which the numerical procedure consists of an iterative exchange of the turbulent flow field as well as the mean density between the CFD code and the subcode solving for the PDF transport equation. The aim is to investigate the impact of the interaction-modelling either on the scalar fields or on the flow and turbulence fields.

3. Configuration and numerical setup

3.1. Configuration

The confined configuration in this study consists of a cylindrical water-cooled chamber of a height of $L=1.2$ m and a diameter of $D=0.5$ m and is supplied with a swirl burner. Geometry data of the nozzle exit of the burner are depicted in Fig. 1. The effective swirl number is found to be $S_{eff}=0.88$, defined by the ratio of tangential to axial momentum flux

$$S_{eff}=\frac{2}{D}\frac{\int_0^R\left(\overline{\rho}\tilde{u}\tilde{w}+\overline{\rho}\widetilde{u''w''}\right)r^2\,\mathrm{d}r}{\int_0^R\left(\rho\tilde{u}^2+\overline{\rho}\widetilde{u''^2}\right)r\,\mathrm{d}r}.\tag{16}$$

With Reynolds numbers based on exit bulk velocities of $Re_{fuel}=8000$ and $Re_{air}=42900$ and a thermal load of $P_{th}=150$ kW the confined flame (TECFLAM case S09C, see [23]) represents an application close to combustion systems of practical importance. Natural gas used as fuel is approximated as methane.

In order to validate the applied models, suitable measurement data obtained with different measuring techniques based on laser-diagnostics are available [23]. The velocity field and correlations are provided by using 2D-Laser-Doppler-Anemometer technique [23,42] and spontaneous Raman scattering was applied for the simultaneous determination of temperature, mixture fraction as well as for the species concentrations. For details, see [3,27].

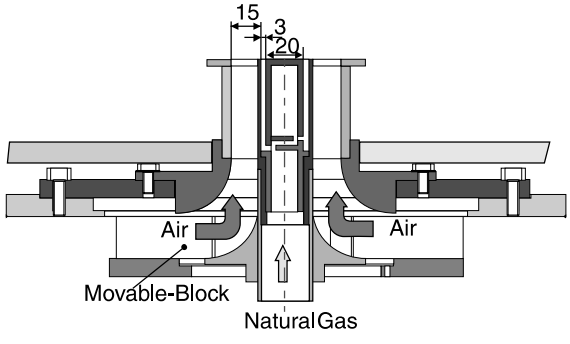

Fig. 1. TECFLAM swirl burner exit geometry and swirl generator.

3.2. Discretisation and solution method

Numerical results are obtained with a two-dimensional elliptic CFD code based on a staggered orthogonal grid and cylindrical coordinates. Correspondingly, an appropriate coordinate transformation of the modelled equations is integrated in the code. Assuming axisymmetry, the half plane of the combustion chamber is discretised by a 80×60 points grid in axial and radial direction, respectively, condensed near the burner and the wall. Numerical methods applied are a QUICK scheme providing second order accuracy for discretisation of the convective terms and a time relaxation scheme in order to achieve stationary solutions. Pressure correction is performed using the SIMPLE algorithm. For the presumed-PDF calculations, the size of the look-up table is approximately 58 MB yielding a sufficient resolution as test calculations have shown.

In order to account for the effects of the interaction-modelling on the flow and scalar fields, only the coupling model is varied while the turbulence models and the chemistry mechanism as described above remain unchanged.

The numerical procedure of the MC-PDF simulations consists of an iterative exchange of information on the turbulent flow field on the one hand and the mean density on the other hand obtained from the finite-volume code and the Monte Carlo subcode with 100 particles used in each computational cell, respectively. For computational efficiency, a local time step method is implemented [24]. In order to enhance the evolution of a stably burning flame, the entire field is initially assumed to be in chemical equilibrium at stoichiometric conditions. The CPU time required is about 140 h on a ALPHA LX533 Linux-workstation. On the other side, it required about 16 h for a stationary solution with the presumed-PDF method (β-PDF) following the procedure described in Section 2.3.1 on the same machine.

3.3. Initial and boundary conditions

The inlet boundary was located at the burner mouth where fuel and air are ejected separately providing well defined boundary conditions. However, since the lowest plane of the LDV measurements was located at $x = 1$ mm above the burner exit, the inlet profiles have been adjusted according to the measurements such that correct volumetric flow rates of fuel and air are matched.

Calculation results can be sensitive to the inlet boundary values, particularly with respect to the dissipation rate, which cannot be directly measured. Though the inlet profile of the dissipation rate can be determined from the given mean velocity and the profile of the turbulent kinetic energy with an assumption of zero axial derivative, it is modelled here with a Prandtl mixing length l proportional to the annulus width R to give $\tilde{\varepsilon} = C_{\mu}^{3/4}\tilde{k}^{3/2}/l$; $l = R/C$ with the constant C to be determined. In our calculations, the values $C = 5$ for the fuel and $C = 50/3$ are used. Standard wall functions are applied approximating the logarithmic law in the boundary layer.

The flame can be characterised by very intensive mixing and combustion processes in the near field of the nozzle. In the reaction zone, being the focus of this work, chemical kinetic effects are significant and the temperature is moderate. Hence, radiation is neglected. This is confirmed by the scatter plots near the centreline as depicted in Fig. 13 ($0 < r < 28$ mm) and Fig. 14 ($0 < r < 45$ mm). The simulations are then carried out under adiabatic conditions, thus neglecting convective and radiative heat loss across the wall. For the accurate prediction of temperature profiles far downstream and in the outer recirculation zone, this simplification can certainly not be applied.

For the composition joint-PDF, the inlet conditions are prescribed as $\boldsymbol{\phi} = (1, 0, 0)$ for the fuel and $\boldsymbol{\phi} = (0, 0, 0)$ for the air. All particles at the inlet are assigned with the same state, respective to their stream, hence, the PDF degenerates to a Dirac function. With regard to the mixture fraction and mass fraction the wall influence on the PDF is modelled by using Neumann conditions for the mean values along with the fact that the turbulence is damped in the cells at the wall. It then follows that the PDF at the wall can be set to a Dirac function assuming zero-gradient conditions for the mean.

4. Results and discussion

Comparisons between experimental data and numerical results obtained with the presumed-PDF model as well as with the MC-PDF model are now presented and discussed.

4.1. Mean flow fields

Figs. 2–4 depict the mean flow field of the swirling flame, calculated with both PDF approaches. Focusing on the near field of the burner, radial velocity distributions are depicted at two different axial positions, $x = 30$ mm and $x = 60$ mm, where x and r denote the axial and radial coordinate, respectively.

Fig. 2 shows the radial distribution of the mean axial velocity $\tilde{u}$. For the lower plane, the profile of $\tilde{u}$ is in good agreement with the experimental data but the intensity of the axial velocity in the central recirculation zone is slightly underestimated. In the axial development of $\tilde{u}$, the profile is shifted outwards, indicating the central recirculation zone being spread as the radial profiles of the radial velocity, Fig. 3, suggest. That the strength of the recirculation is not fully captured can be claimed to

the turbulent transport. Besides known problems with boundary conditions, it then appears that the assumption of equilibrium turbulence in the turbulence model used is violated in this region of the complex flow [9,35], where non-equilibrium effects are present.

A similar picture is revealed for the mean tangential velocity $\tilde{w}$, depicted in Fig. 4. It can be seen that the magnitude of $\tilde{w}$ is hardly influenced by the broadened shape of the flame. This indicates correct boundary conditions for the tangential velocity component that is mainly responsible for the flux of tangential momentum, and thus swirl intensity. The same deviations between measured and computed flow fields could be observed for the isothermal case as test calculations have shown.

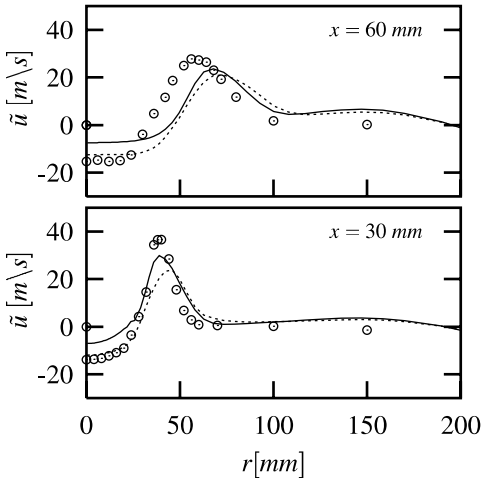

Fig. 2. Radial distribution of mean axial velocity $\tilde{u}$ at $x = 30$ mm and $x = 60$ mm (— β-PDF, ··· MC-PDF, ⊙ Exp).

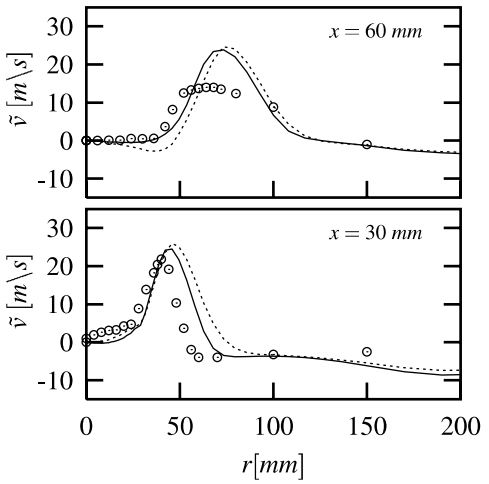

Fig. 3. Radial distribution of mean radial velocity $\tilde{v}$ at $x = 30$ mm and $x = 60$ mm (— β-PDF, ··· MC-PDF, ⊙ Exp).

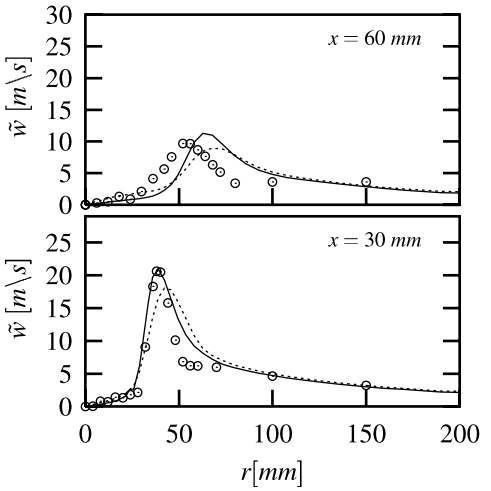

Fig. 4. Radial distribution of mean tangential velocity $\tilde{w}$ at $x = 30$ mm and $x = 60$ mm (— β-PDF, ··· MC-PDF, ⊙ Exp).

Whilst the Monte Carlo results are similar to those with the presumed-PDF discussed above, it appears that the results for the turbulent quantities, here the mean turbulent kinetic energy $\tilde{k}$ presented in Fig. 5 as a measure of turbulence intensity, differ. The energy $\tilde{k}$ is underestimated in the lower part of the flame by the presumed-PDF whilst a satisfactory agreement with experimental data is shown by MC-PDF. A better description of the chemistry in the latter well accounts for the influence of the combustion on the characteristics of the flow through a better capture of the density variation. Additionally, the critical shear stresses $\widetilde{u''v''}$ and $\widetilde{u''w''}$ are presented in Figs. 6 and 7.

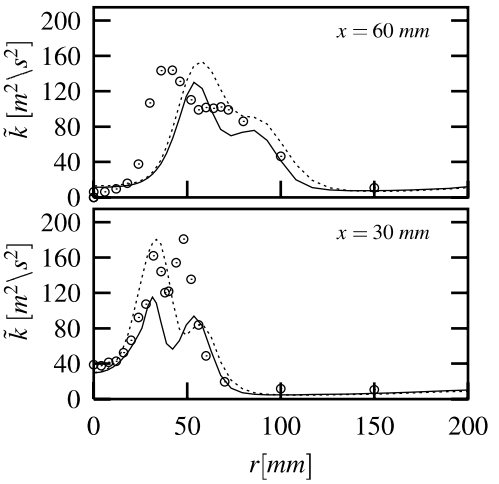

Fig. 5. Radial distribution of mean turbulent kinetic energy $\tilde{k}$ at $x = 30$ mm and $x = 60$ mm (— β-PDF, ··· MC-PDF, ⊙ Exp).

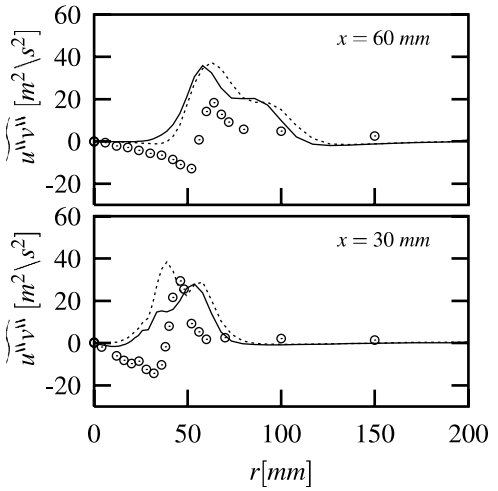

Fig. 6. Radial distribution of Reynolds stress component $\widetilde{u''v''}$ at $x = 30$ mm and $x = 60$ mm (— β-PDF, ··· MC-PDF, ⊙ Exp).

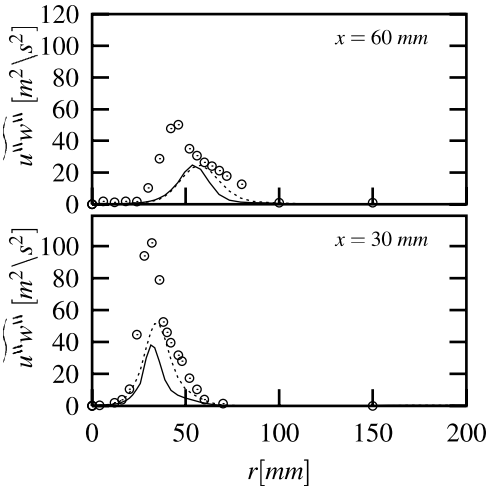

Fig. 7. Radial distribution of Reynolds stress component $\widetilde{u''w''}$ at $x = 30$ mm and $x = 60$ mm (— β-PDF, ··· MC-PDF, ⊙ Exp).

4.2. Species concentrations

In this section, distributions of major and minor species are discussed at the axial position $x = 40$ mm, since no experimental data are available at $x = 30$ mm.

Fig. 8 depicts the mean and rms-values of mixture fraction, $\tilde{f}$ and $(\widetilde{f''^2})^{0.5}$. Comparing the profiles obtained with the β-PDF approach to the experimental data shows $\tilde{f}$ being overpredicted in the inner mixing layer. This indicates an oversupply of fuel caused by underpredicted turbulent mixing. This tendency is not confirmed by the MC-PDF simulation. Satisfactory agreement of the β-PDF with the MC-PDF results can be observed for the profiles of rms-values of mixture fraction.

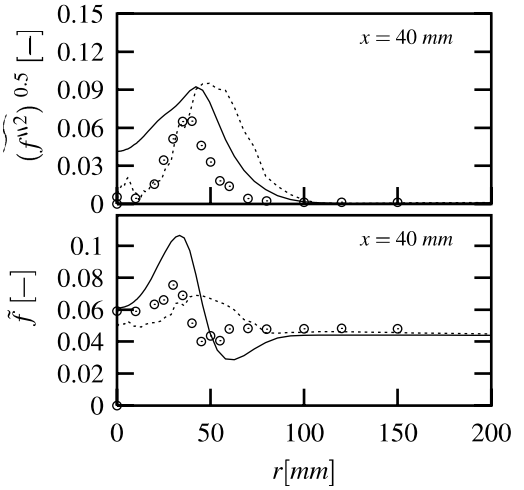

Fig. 8. Radial distribution of mean and rms-values of mixture fraction f at $x = 40$ mm (— β-PDF, ··· MC-PDF, ⊙ Exp).

Mean and rms-data of the mass fraction of CO_2 are depicted in Fig. 9. The profile of the distribution of $\tilde{Y}_{CO_2}$ calculated with the presumed-PDF model is in good agreement with the experiment as well as with the MC-PDF. Although the variance $\widetilde{Y''^2_{CO_2}}$ is underpredicted, the profile is in qualitative accordance with the MC-PDF result. A similar distribution is found for the second reaction progress variable, Y_{H_2O}, though not shown here. Considering the fact that the chemical source terms of Eqs. (4) and (5) involve significant modelling in the

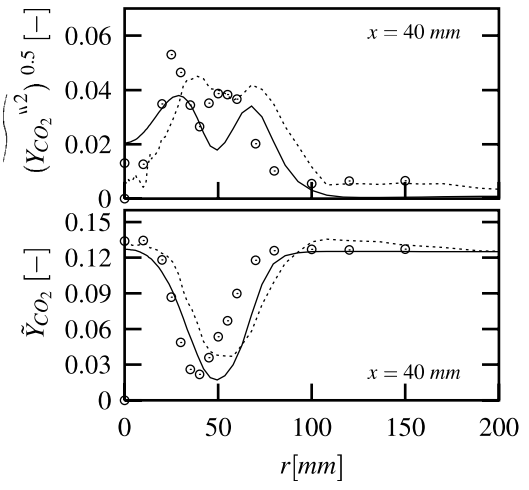

Fig. 9. Radial distribution of mean and rms-values of mass fraction Y_{CO_2} at $x = 40$ mm (— β-PDF, ··· MC-PDF, ⊙ Exp).

frame of presumed-PDF approaches, the overall agreement of the profiles with the experiment is satisfying.

As representatives of major and minor species, mean mass fractions of CH_4 and CO are shown in Fig. 10. The mass fraction $\tilde{Y}_{CH_4}$ is slightly overestimated in the inner mixing zone where fuel is mixed into the flow. In this case, the MC-PDF calculation does not confirm the β-PDF uniquely. A comparison of $\tilde{Y}_{CO}$ depicted in the top of Fig. 10 leads to a different picture. The agreement of the sensitive quantity $\tilde{Y}_{CO}$ with the experiment is very satisfactory for the presumed-PDF model. Taking into consideration an uncertainty in CO-measurements of about 20%, the deviations between both models remain acceptable, especially around the reaction zone region.

4.3. Statistical analysis

The statistical analysis aims at the question whether the loss of statistical information in the assumptions involved in the construction of the multivariate presumed-PDF is reasonable. For this purpose, the same joint-PDF is constructed in a post-processing step using the single particle information of the MC-PDF simulation as parameters of the β-functions. Then, the integration according to Eq. (10) is carried out using the calculated one-dimensional PDFs, denoted as MC-β-PDF. By leaving the flow field unchanged, the investigation with MC-β-PDF concentrates on the prediction of species concentrations and temperature. The comparison of these results with the simulation results obtained by using the full MC-PDF simulation is discussed below.

Fig. 11 shows results of the full MC-PDF simulation and the constructed MC-β-PDF integration at the (additional) axial location $x = 20$ mm. In the bottom pic-

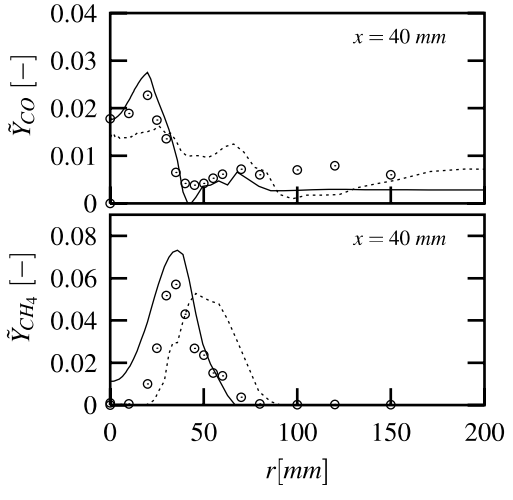

Fig. 10. Radial distribution of mean mass fractions $\tilde{Y}_{CH_4}$ and $\tilde{Y}_{CO}$ at $x = 40$ mm (— β-PDF, ··· MC-PDF, ⊙ Exp).

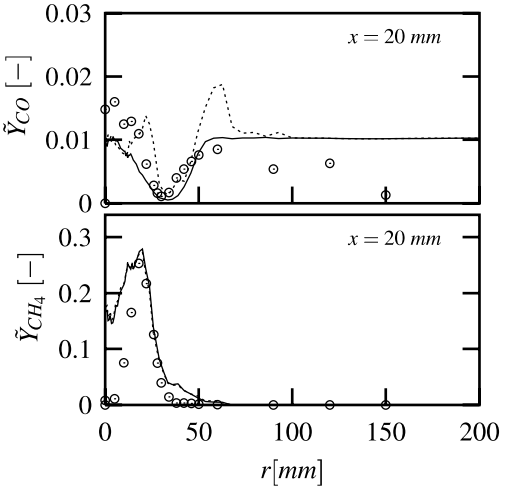

Fig. 11. Radial distribution of mean mass fractions $\tilde{Y}_{CH_4}$ and $\tilde{Y}_{CO}$ at $x = 20$ mm (— MC-PDF, ··· MC-β-PDF, ⊙ Exp).

ture, both solutions yield almost identical results for $\tilde{Y}_{CH_4}$. This indicates the insensitivity of the major species $\tilde{Y}_{CH_4}$ with respect to the chosen PDF construction approach. In the upper part of Fig. 11, both solutions differ especially outside the reaction zone which demonstrates the expected loss of statistical information. In spite of the observed deviations, the level of CO concentration is sufficiently better predicted with MC-PDF method than with presumed ansatz. If additionally the results in Fig. 10 are taken into consideration, it appears that the minor species are sensitive to the chosen PDF approach. Hence, the numerical efficiency alone seems to prove the attractiveness of the multivariate presumed-PDF approach to capture finite-chemistry effects in complex flames.

4.4. Scatter plots and local extinction

An inherent feature of the MC-PDF method is the ability to describe local extinction effects because it contains the full statistical information. Furthermore, it allows to obtain detailed information about the thermochemical flame state and the effects of chemistry–turbulence interaction. A quantitative comparison in terms of conditional means is already addressed in [13]. Here we only aim to qualitatively demonstrate how the Monte Carlo simulation in combination with ILDM chemistry allows to take finite-chemistry effects into account.

For the investigation of local extinction effects, single shot data of the Raman measurements provide a valuable basis. The instantaneous information at a certain location give insight into the finite-chemistry effects of the flame. For this purpose, the radius is separated into four zones as sketched in Fig. 12. The most inner region

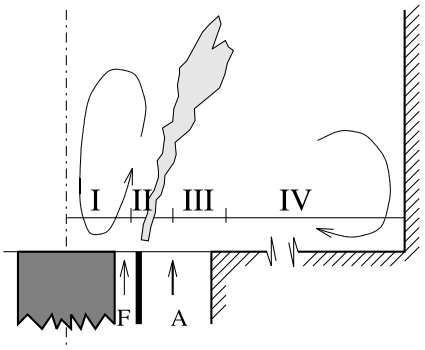

	$x = 10$ mm	$x = 40$ mm	Comment
I	$0 < r < 18$ mm	$0 < r < 25$ mm	Inner Recirculation Zone
II	$22 < r < 28$ mm	$30 < r < 45$ mm	Mixing Zone with Fuel
III	$30 < r < 36$ mm	$50 < r < 60$ mm	Mixing Zone with Air
IV	$40 < r < 120$ mm	$70 < r < 100$ mm	Outer Recirculation Zone

Fig. 12. Classification of radial ranges with respect to their characteristic phenomena (F: fuel, A: air).

(I) lies within the recirculation zone. The second and third section can be considered as regions of strong mixing being controlled either by fuel (II) or air (III). Section 4 is featured by the outer recirculation zone.

The qualitative comparisons in Figs. 13 and 14 yield a good agreement in particular near the centreline. The effects of finite-chemistry interaction become very apparent in regions I and II at $x = 10$ mm. In the inner of region I, stoichiometric and slightly rich mixtures ($f_{st} = 0.055$) with high temperature prevail. Furthermore, most of the data points which are scattered indicate that the gas has completely reacted and that no significant temperature loss occurred. According to that, the heat loss due to radiation and convection can be neglected in this region, in which hot combustion products are transported from flame regions further downstream back to the burner mouth. This can be suggested by means of the axial velocity profiles in Fig. 2. Further outside of the region I, samples with a wide spread in mixture fraction can be seen ranging almost from pure air ($f = 0$) to pure fuel ($f = 1$). As shown in Fig. 12, this region lies above the fuel and air nozzles; therefore the results reflect the different states of mixing. The temperatures are roughly divided into two branches: one at ambient temperature, that means unreacted mixtures, and the other close to the reacting temperature. In the simulation, the temperature of the samples in region I is uniformly distributed and, hence, emphasise kinetic effects contrary to experiments which show greater evidence of bimodality. As can be seen, the comparison between the calculated and measured results reveals some significant deviations. These point out that the turbulence modelling assumption based on equilibrium turbulence is unable to account for non-equilibrium turbulence effects in this region. In fact, between regions I and II very strong shear rates are present and affect the turbulence and mixing process in the inner recirculation zone.

In particular in region II at $x = 10$ mm, ignitable mixtures around $f_{st} = 0.055$ with a temperature of 300–400 K are detected in both, the experiment and the simulation. The chemical reaction is prevented by the high flow velocities and a too small heat and mass transfer from the inner recirculation zone. This indicates that the strong turbulence yields premixed conditions but suppresses the reaction to take place.

The reaction progress becomes apparent by a comparison of the scatter plots at $x = 10$ mm and $x = 40$ mm for the centre of the flow. The mixture fraction range becomes narrow reflecting the rapid mixing in the flow. At $x = 40$ mm, the different flame regimes mentioned above can still be distinguished and the thermochemical state from the inner and the outer recirculation zone has hardly changed in comparison to $x = 10$ mm. However, in the mixing region of the fuel and air streams the temperatures now cover the whole range from 300 to 2300 K. The samples with intermediate temperatures can have different histories [27]: (1) They stem from local flame extinction leaving the gas in a partially reacted state. Local flame extinction certainly occurs in this flame and has been observed by visual inspection. (2) They are compositions of hot burnt gas and cold air/fuel mixtures which have not yet completely reacted.

In region III, deviations between experiments and the simulation become more apparent at both axial planes. The temperatures measured are considerably below the adiabatic results of the simulation. Hence, the heat loss and exchange with colder gases of the outer recirculation

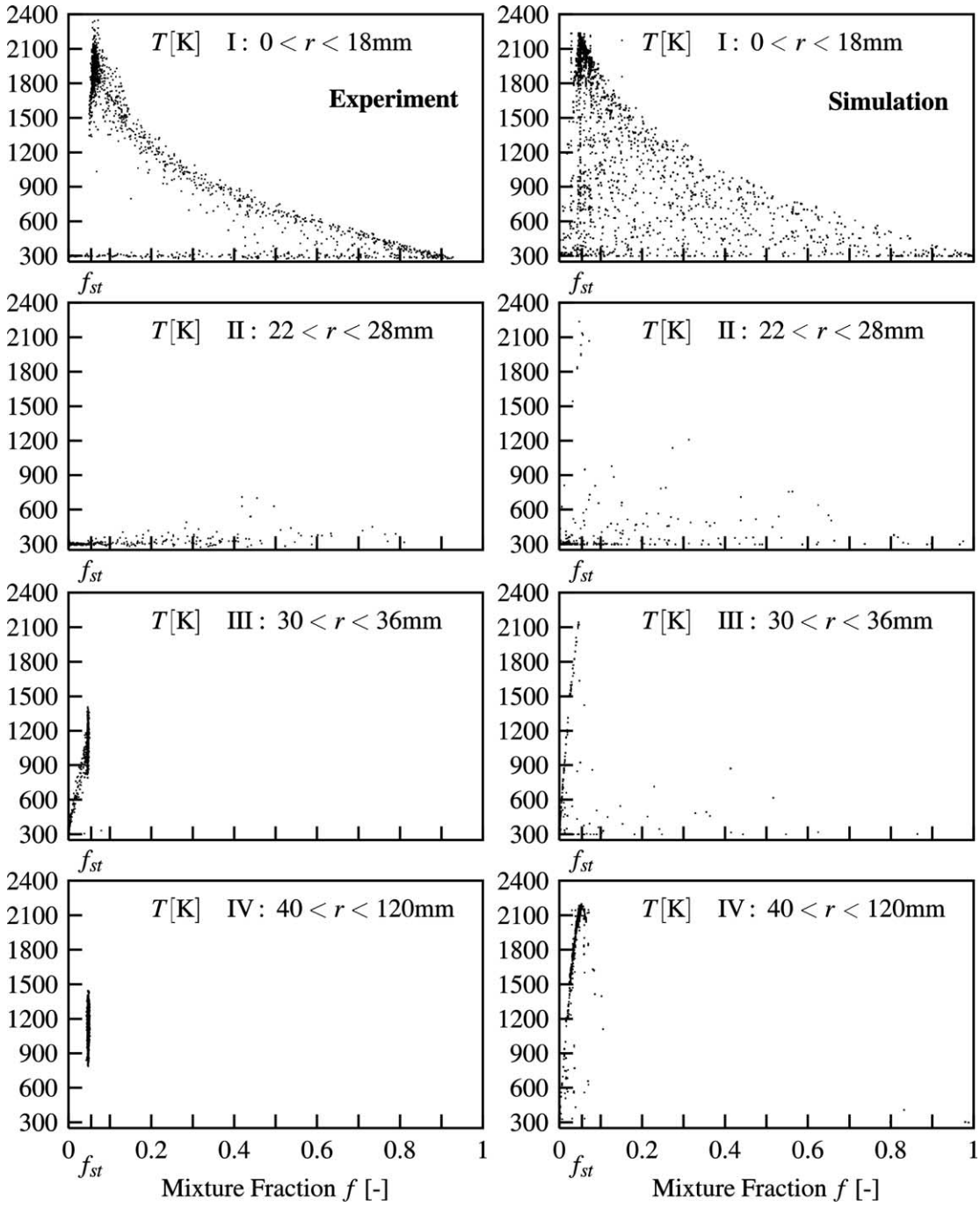

Fig. 13. Scatter plots of temperature at $x = 10$ mm.

zone play an important role. In this outer zone, the heat loss leads to a lower temperature range of 800–1400 K. It is remarkable that the experiments show almost no fluctuations in the mixture fraction in the outer region indicating a very homogeneous state.

5. Conclusions

The present work was focused on the application of PDF methods (presumed-PDF model and Monte Carlo-scalar-PDF method) with regard to their effects on the

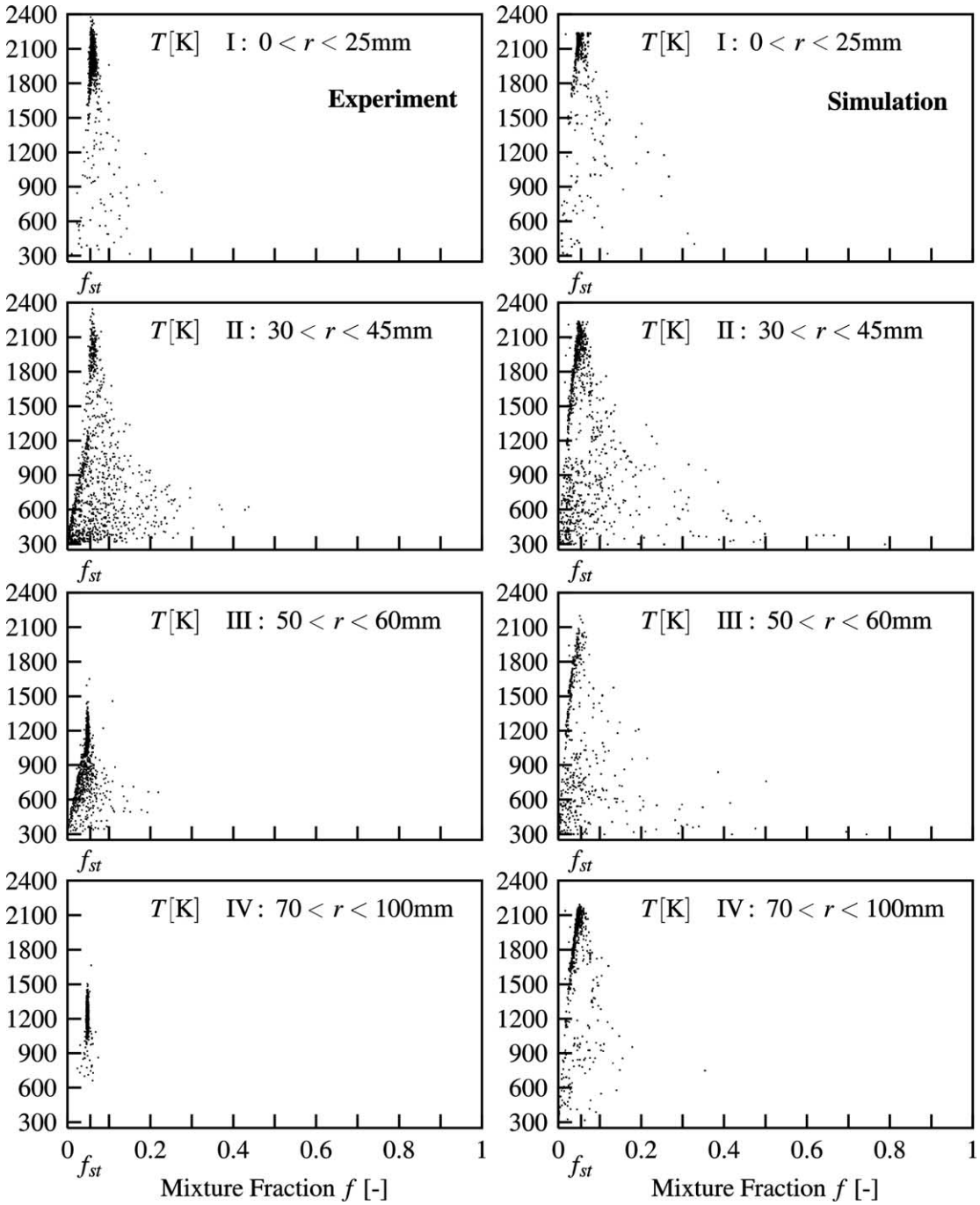

Fig. 14. Scatter plots of temperature at $x = 40$ mm.

prediction capability of a confined strongly swirling flame as it appears in combustion systems of technical importance.

Simulations with the presumed-PDF model are carried out in combination with a reduced chemistry mechanism based on the ILDM-method capturing chemical non-equilibrium effects. Comparisons with experimental data have shown that the main features of the flow and mixing fields are well predicted accompanied by an overestimated spreading of the central

recirculation zone in the axial course of the flame. Computed distributions of major species mass fractions as well as of the corresponding variances are in reasonable accordance with measured profiles. Likewise is the concentration of CO as one of the minor species being sensitive to chemical kinetics.

Comparisons with calculations carried out with the MC-PDF method confirm the presumed-PDF model. Deviations between both methods can be explained with reduced statistical information about the PDF of the presumed-PDF model. Through a statistical analysis of the MC-PDF data, the assumption leading to the construction of the joint-PDF via one-dimensional β-functions is shown to be permissible for such applications. Therefore, together with a generated look-up table, the multivariate presumed-PDF model represents a very attractive method to capture finite-chemistry effects in complex combustion configurations. Of course, including a more elaborate ansatz can academically improve the assessments.

The computational effort between the presumed-PDF model and the MC-PDF method differs significantly. The CPU time required for a stationary solution using the presumed-PDF model is about 16 h on a ALPHA LX533 machine. A MC-PDF simulation with a full coupling of the CFD code and the Monte Carlo procedure rises up to 140 h. However, it provides a good tool to distinguish effects of the chemistry and the turbulence models. This numerical efficiency was also the major motivation for the presented approach.

Acknowledgements

This work has been carried out in the framework of the DFG project JA 544/13-1. The authors wish to thank the Deutsche Forschungsgemeinschaft (DFG) for the financial support.

References

[1] M.S. Anand, A.T. Hsu, Calculations of swirl combustors using joint velocity–scalar probability density function method, AIAA 35 (7) (1997) 1143–1150.

[2] H. Barths, N. Peters, N. Brehm, M. Pfitzner, V. Smiljanovski, Simulation of pollutant formation in a gas-turbine combustor using unsteady flamelets, in: Twenty-Seventh Symposium (International) on Combustion, The Combustion Institute, 1998, pp. 1841–1847.

[3] V. Bergmann, W. Meier, D. Wolff, W. Stricker, Application of spontaneous Raman and Rayleigh scattering and 2D LIF for the characterization of a turbulent $CH_4/H_2/N_2$ jet diffusion flame, Appl. Phys. B 66 (1996) 489–502.

[4] R.-W. Bilger, Conditional moment closure for turbulent reacting flow, Phys. Fluids A 5 (2) (1993) 436–444.

[5] J.-Y. Chen, W. Kollmann, R.W. Dibble, Pdf modeling of turbulent nonpremixed methane jet flames, Combust. Sci. Technol. 64 (1989) 315–346.

[6] S.-M. Correa, Power generation and aeropropulsion gas turbines: from combustion science to combustion technology, in: Twenty-Seventh Symposium (International) on Combustion, The Combustion Institute, 1998, pp. 1793–1807.

[7] S.M. Correa, M.C. Drake, R.W. Pitz, W. Shyy, Prediction and measurement of a non-equilibrium turbulent diffusion flame, in: Twentieth Symposium (International) on Combustion, The Combustion Institute, 1984, pp. 337–343.

[8] B.-J. Daly, F.-H. Harlow, Transport equations in turbulence, Phys. Fluids 13 (1970) 2634–2649.

[9] G. Früchtel, Untersuchungen zur Gleichgewichtshypothese in verdrallten reagierenden Strmungen, Ph.D. Thesis, Technische Hochschule Darmstadt, 1997.

[10] G.-M. Goldin, S. Menon, A comparison of scalar pdf turbulent combustion models, Combust. Flame 113 (1998) 442–453.

[11] E. Gutheil, H. Bockhorn, The effect of multi dimensional pdf's on the turbulent reaction rate in turbulent reacting flows at moderate Damköhler numbers, PhysicoChem. Hydrodyn. 9 (3/4) (1987) 525–535.

[12] A. Hinz, Numerische Simulation turbulenter Methan-Diffusionsflammen mittels Monte Carlo PDF Methoden, Ph.D. Thesis, Technische Universität Darmstadt, 2000.

[13] A. Hinz, T. Landenfeld, E.P. Hassel, J. Janicka, Advanced modeling of turbulent non-equilibrium swirling natural gas flames, in: 4th International Symposium on Engineering Turbulence Modelling and Measurements, Corsica, Elsevier, Amsterdam, 1999, pp. 831–840.

[14] T. Hulek, R.P. Lindstedt, Computations of steady-state and transient premixed turbulent flames using pdf methods, Combust. Flame 104 (1996) 481–504.

[15] J. Janicka, W. Kolbe, W. Kollmann, Closure of the transport equation for the probability density function of turbulent scalar fields, J. Non-Equil. Thermodyn. 4 (1979) 47–66.

[16] J. Janicka, W. Kollmann, A two-variables formalism for the treatment of chemical reactions in turbulent H_2–air diffusion flames, in: Seventeenth Symposium (International) on Combustion, The Combustion Institute, 1978, pp. 421–430.

[17] W.-P. Jones, Turbulence modeling and numerical solution methods for variable density flows, in: P.A. LibbyF.A. Williams (Eds.), Turbulent Reacting Flows, Academic Press, New York, 1994, pp. 309–347.

[18] W.P. Jones, M. Kakhi, PDF modeling of finite-rate chemistry effects in turbulent non-premixed jet flames, Combust. Flame 115 (1998) 211–229.

[19] W.-P. Jones, P. Musonge, Closure of the Reynolds stress and scalar flux equations, Phys. Fluids 31 (12) (1988) 3589–3604.

[20] A.R. Kerstein, A linear-eddy model of turbulent scalar transport and mixing, Combust. Sci. Technol. 60 (1988) 391–421.

[21] T. Landenfeld, Numerische Beschreibung turbulenter Methandiffusionsflammen mit Schließ ungsmodellen zweiter Ordnung und angenommenen Wahr-

scheinlichkeits dichtefunktionen, Ph.D. Thesis, Technische Universität Darmstadt, 1999.
[22] T. Landenfeld, A. Hinz, J. Janicka, Statistical analysis of reactive scalars in a turbulent diffusion flame using Monte Carlo pdf method, in: Joint Meeting of the British, German and French Sections, Nancy, The Combustion Institute, 1999, pp. 1–3.
[23] T. Landenfeld, A. Kremer, E.-P. Hassel, J. Janicka, T. Schäfer, J. Kazenwadel, C. Schulz, J. Wolfrum, Laser-diagnostic and numerical study of strongly swirling natural gas flames, in: Twenty-Seventh Symposium (International) on Combustion, The Combustion Institute, 1998, pp. 1023–1030.
[24] A. Laxander, Numerische Simulation von turbulenten Diffusionsflammen mit einem PDF-Transportgleichungsmodell, Ph.D. Thesis, Universität Stuttgart, 1996.
[25] P.A. Libby, F.A. Williams, Turbulent Reacting Flows, Academic Press, New York, 1994.
[26] U. Maas, S.-B. Pope, Implementation of simplified chemical kinetic based on intrinsic low-dimensional manifolds, in: Twenty-Fourth Symposium (International) on Combustion, The Combustion Institute, 1992, pp. 103–112.
[27] W. Meier, O. Keck, B. Noll, O. Kunz, W. Stricker, Investigations in the TECFLAM swirling diffusion flame: laser Raman measurements and CFD calculations, Appl. Phys. B 71 (2000) 725–731.
[28] N. Peters, Laminar flamelet concepts in turbulent combustion, in: Twenty-First Symposium (International) on Combustion, The Combustion Institute, 1986, pp. 1231–1250.
[29] N. Peters, Turbulent Combustion, Cambridge University Press, Cambridge, 2000.
[30] D. Pfuderer, A. Neuber, G. Früchtel, E.P. Hassel, J. Janicka, Turbulence modulation in jet diffusion flames: modeling and experiments, Combust. Flame 106 (1996) 301–317.
[31] H. Pitsch, M. Chen, N. Peters, Unsteady flamelet modeling of turbulent hydrogen–air diffusion flames, in: Twenty-Seventh Symposium (International) on Combustion, The Combustion Institute, 1998, pp. 1057–1064.
[32] S.B. Pope, A Monte Carlo method for the pdf equations of turbulent reactive flow, Combust. Sci. Technol. 25 (1981) 159–174.
[33] S.B. Pope, Pdf methods for turbulent reactive flows, Prog. Energy Combust. Sci. 11 (1985) 119–192.
[34] S.B. Pope, New developments in pdf modelling of nonreactive and reactive turbulent flows, in: T.W.J. PeetersK. Hanjalić (Eds.), 2nd International Symposium on Turbulence, Heat and Mass Transfer, 1997, pp. 35–45.
[35] A. Sadiki, Thermodynamik und Turbulenzmodellierung, Habilitationsschrift, Technische Universität Darmstadt, 1998.
[36] S. Subramaniam, S.B. Pope, A mixing model for turbulent reactive flows based on euclidean minimum spanning trees, Combust. Flame 115 (1998) 487–514.
[37] L. Valiño, C. Dopazo, A binomial langevin model for turbulent mixing, Phys. Fluids A 3 (12) (1991) 3034–3037.
[38] D. Schmidt, J. Segatz, U. Riedel, J. Warnatz, U. Maas, Simulation of laminar methane–air flame using automatically simplified chemical kinetics, Combust. Sci. Technol. 113–114 (1996) 3–16.
[39] U. Maas, Mathematically modeling of the coupling of chemical kinetics with flow and molecular transport, in: Scientific Computing in Chemical Engineering II, Springer, Heidelberg, 1999, pp. 26–56.
[40] R. Bender, T. Blasenbrey, U. Maas, Coupling of detailed and ILDM-reduced chemistry with turbulent mixing, in: 28th Symposium (International) on Combustion, 2000, pp. 101–106.
[41] R.P. Lindstedt, S.A. Louloudi, E.M. Vaos, Joint PDF modeling of pollutant formation in piloted turbulent jet diffusion flames with comprehensive chemistry, in: 28th Symposium (International) on Combustion, 2000, pp. 149–156.
[42] C. Schneider, S. Repp, A. Sadiki, A. Dreizler, J. Janicka, The effect of swirling number variation on turbulent transport and mixing processes in swirling recirculating flows: experimental and numerical investigations, in: 2nd International Symposium on Turbulence and Shear Flow Phenomena, 2001, pp. 363–368.